The (2-0) R(0) and R(1) transition frequencies of HD determined to a 10 -10 relative accuracy by Doppler spectroscopy at 80 K

Samir Kassi, Clément Lauzin, Justin Chaillot, Alain Campargue

The (2-0) *R*(0) and *R*(1) transition frequencies of HD determined to a 10^{-10} relative accuracy by Doppler spectroscopy at 80 K

Samir Kassi [a], Clément Lauzin [b], Justin Chaillot [a], Alain Campargue [a*]

The Doppler broadened *R*(0) and *R*(1) lines of the (2-0) vibrational band of HD have been measured at liquid nitrogen temperature and at pressures of about 2 Pa, with a comb referenced continuous-wave cavity ring-down spectrometer set-up. Transition frequencies of 214905335185 and 217105181898 kHz were derived from 33 and 83 recordings, with corresponding root mean squared deviation of 53 and 33 kHz for the *R*(0) and *R*(1) transition, respectively. This is the first sub-MHz frequency determination of the *R*(0) transition frequency and represents a three order of magnitude accuracy improvement compared to literature. The *R*(1) transition frequency is in very good agreement with previous determinations in saturation regime reported with similar accuracy. To achieve such accuracy, the transition frequency of a (101)-(000) 2_{11}-3_{12} line of $H_2{}^{16}O$ interfering with the *R*(0) line had to be precisely determined and is reported with a standard error of 100 Hz at 214904329820.80(10) kHz (relative uncertainty of 5×10^{-13}). These measurement sets provide stringent reference values for validating future advances in the theoretical description of the hydrogen (and water) molecule.

[a] *Univ. Grenoble Alpes, CNRS, LIPhy, 38000 Grenoble, France*
[b] *Institute of Condensed Matter and Nanosciences (IMCN), Université Catholique de Louvain, Louvain-la-Neuve, Belgium*
* Corresponding author: E-mail: alain.campargue@univ-grenoble-alpes.fr

Introduction

Due to its relative simplicity, the dihydrogen molecule is of fundamental interest in physics and chemistry. The HD isotopologue which represents the simplest neutral heteronuclear diatomic molecule has been at the origin of a fruitful scientific emulation on both theoretical (*e.g.* [1], [2], [3], [4]), and experimental (*e.g.* [5], [6], [7], [8], [9], [10], [11], [12], [13], [14], [15], [16], [17], [18], [19]) fronts.

Although weak, the rovibrational transitions in HD are about two orders of magnitude stronger than in H_2. This is due to the existence of a small electric dipole moment in HD, giving rise to allowed electric dipole transitions which are strictly forbidden in H_2 (and D_2), in which only electric quadrupole transitions remain observable. The electric dipole transitions in HD are thus particularly suitable to achieve very high accuracy frequency determination using absorption spectroscopy. Since the pioneering work of Herzberg [5], the weak HD absorption spectrum has been extensively studied using a variety of experimental techniques (see the review of experimental measurements up to 2016 included in Table 1 of [14]). Overall, more than seventy transitions were detected from the rotational spectrum [11] up to the fifth overtone band, (6–0) near 520 nm [8].

While the pioneer experimental efforts were motivated by planetary applications, the HD molecule has become a benchmark system which triggered great efforts to improve quantum physics calculation accuracy. This includes in particular quantum electrodynamics corrections (QED) of the energy levels up to the sixth order [20], [3] and hyperfine splitting determination [21], [4], [22]. Interestingly, HD is for now the sole dihydrogen isotopologue for which a disagreement exists on the dissociation energy between experimental and theoretical values [23], [13], [3]. HD is thus an attractive molecular candidate to challenge further theoretical predictions and test the amplitude of the QED corrections.

Experimental advances in terms of sensitivity, resolution and accuracy on the frequency determination of HD rovibrational transitions, ionization potential and dissociations energies provide stringent validation tests of the most advanced calculations [23], [13].

Doppler broadening is a strong limitation factor to achieve sub-MHz precision on line center determination, even at low temperature. Indeed, the full width at half maximum (FWHM) of the Doppler limited profile of the (2-0) $R(0)$ or $R(1)$ HD lines is about 700 MHz at 80 K. Saturation spectroscopy provides a powerful tool to circumvent Doppler broadening. Recently, accurate measurements of HD transitions were reported in the sub-Doppler regime using either action spectroscopy schemes [24], [18] or the power enhancement of a Fabry Perot cavity to observe Doppler free Lamb dip signatures [15], [25]. In particular, the Hefei [15] and Amsterdam [25] groups retrieved (2-0) $R(1)$ transition frequencies from Lamb dips exhibiting a dispersive-like spectral structure. The initial reported values differed by 900 kHz, a difference significantly larger than the combined error bar of the two measurements. This discrepancy and the unusual Lamb dip profile were examined in two subsequent studies led by the same groups [16], [26]. In Hefei, an experimental study was performed with an enhanced signal-to-noise ratio

and the use of different spectroscopic techniques confirming the dispersive-like shape, fitted with a Fano profile [26]. Physical mechanisms at the origin of this Fano-type profile was very recently discussed by the same group [27]. For the Amsterdam group, the dip was fitted according to Bloch equations formalism and introducing crossovers transitions [16]. Both groups found line positions in agreement with each other within the error bars of 50 and 240 kHz for Amsterdam and Hefei, respectively.

Interestingly, the same (2-0) $R(1)$ transition was measured with similar accuracy in Doppler regime at room temperature in Caserta [19] providing an error bar of 76 kHz, on the same order as the one of Doppler free measurements. The line position of the (2-0) $R(1)$ is now determined within 50 kHz but the origin of the observed dispersive Lamb-dip profile remains a subject of discussion.

In the present work, we report on high accuracy frequency measurements of the $R(0)$ and $R(1)$ transitions of the (2-0) vibrational band of HD at liquid nitrogen temperature (about 80 K). The advantages of cooling are several: *(i)* the Doppler broadening is reduced by about a factor of two, *(ii)* the intensity of the $R(0)$ transition is increased by a factor of about 3, compared to its 296 K value, the intensity of the $R(1)$ transition being mostly unchanged, *(iii)* spectral interferences with lines due to impurities, water in particular, are minimized since vapor pressure of most contaminants are drastically reduced. Note that while the (2-0) $R(1)$ transition frequency was determined by three groups with an accuracy better than 100 kHz, the best-to-date frequency determination of the (2-0) $R(0)$ transition is 30 MHz [12]. The lack of accurate measurements of the $R(0)$ line is related to the proximity of a 10^5 times more intense water line which precludes room temperature experiments. Our experimental approach for high accuracy HD measurements at low pressures in a water free environment is described in the next section. It combines the advantages of *(i)* a very monochromatic and stable laser source ($\Delta\nu$~100Hz, drift=1Hz/s) developed for cavity ring-down spectroscopy (CRDS) cavity [28], [29], *(ii)* an absolute frequency calibration provided by a frequency comb and *(iii)* a CRDS cell cooled down to liquid nitrogen temperature. In Section 3, we present the transition frequency determination including a discussion of the possible impact of the hfs structure on the retrieved line centers and the error budget. The obtained transition frequencies are discussed in relation with literature results in Section 4, before the Concluding remarks (Section 5).

Experiment

The spectra were recorded at the Université Grenoble Alpes with a set-up presented in **Fig. 1**. The figure is structured in three blocks, from top to bottom, those concern (1) the frequency calibration, (2) the light source and (3) the cavity ring-down spectrometer probing a gas cell working at liquid nitrogen temperature. The VCOF light source is a DFB laser diode locked through optical feedback to a highly-stable V-shaped cavity [28], [29], [30]. This source has sub-kHz emission line width, typically 10 mW output power, and exhibits a maximum frequency drift of 7 Hz/s [30], [31]. Its frequency is first roughly determined using a wavemeter (Burleigh, 50 MHz resolution) and refined using a self-referenced frequency comb from Menlo. The repetition rate (250 MHz) and carrier offset frequencies (20 MHz) of

the comb are phase locked to a 10 MHz GPS disciplined Rb oscillator (GPS-RbO) with a relative frequency stability $\Delta\nu/\nu=2\times10^{-12}$ limited by the GPS accuracy. The design of the continuous-wave cavity ring-down spectrometer (CW-CRDS) follows mainly the one presented in [28]. The spectrometer has been slightly modified by the addition of a pair of optical amplifiers (Thorlabs BOA 1036P, Thorlabs BOA 1410P). The very stable laser source is made tunable over 18 GHz range using a single side-band generator, the Mach-Zender modulator (MZM) in **Fig. 1**, driven by a frequency synthesizer (SMF 100A, Rohde&Schwarz), referenced to the GPS-RbO.

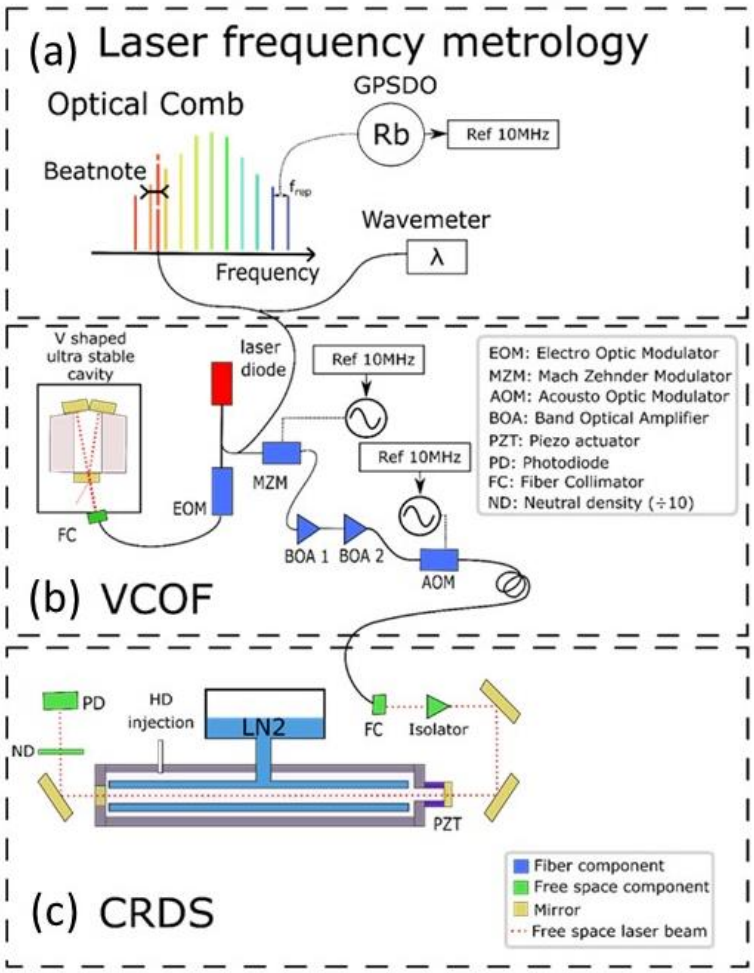

FIG. 1.
Experimental set-up developed in Grenoble. The figure is structured in three blocks, detailing from top to bottom, (a) the frequency calibration, (b) the light source and (c) cavity ring-down spectrometer, respectively. GPSDO stands for GPS Disciplined Oscillator, VCOF stands for V-shaped Cavity-Based Optical Feedback and LN2 for liquid nitrogen. The Acousto-Optic Modulator AOM is driven at 88.5 MHz.

The gas sample, HD (from ISOTEC with 98 % and 99.3% stated isotopic and chemical purity, respectively), was injected through a computer controlled electro-valve and the pressure monitored with a 1 Torr gauge (Baratron model 626B). A weak flow was set through a 10 turns needle valve connecting the cell to a turbo pump group. The pressure was actively regulated to 2 Pa using a computer based Proportional/Integral controller. The design of the cell is very close to the one reported in [32], [33]. It is composed of three concentric stainless steel cylinder cell surrounding the gas sample. The external

stainless-steel cylinder is 1.4 m long, with a diameter of d = 63 mm, while the cryostat is made of the two inner co-axial tubes (d = 1.6 and 2 cm), welded at each end by a hollow disc to form a reservoir. It is suspended at its center by a jacketed 2 cm diameter tube used to fill the cryostat with liquid nitrogen. The main difference with [32] is that the mirrors can be further aligned while the cell is put under vacuum and cooled down. The enhanced conduction of HD compared to CH_4 studied in previous works [32], [34], [35] forced us to work at very low pressure (2 Pa) to prevent any excessive cooling of the external part of the cell.

During recording, the optical frequency is dynamically adjusted by subtracting an adjustable microwave frequency between 2 and 20 GHz using the MZM. To speed up the recording, the spectra are acquired in an interlaced manner with frequency hopping bursts equal to the free spectral range of the CRD cavity. The cavity modes are thus systematically resonant. To increase the resolution, an intermediate optical frequency is chosen inducing a procedure of relock of the CRDS cavity modes, thanks to the PZT mounted mirror. Another burst is then recorded. Thus 4 series of spectra are interlaced to reach a resolution of 25 MHz with a cavity whose FSR is 100 MHz. A full spectrum, with 10 to 40 RD per spectral point, is recorded within typically 1 minute.

Results

The R(1) line

The $R(1)$ transition, already accurately measured in [15], [25], [26] and [19] was used to validate our measurement procedure. Eighty-three fourfold interlaced spectra were recorded at liquid nitrogen temperature with frequency step of 100 MHz (matching the CRDS cavity free spectral range) leading to a final 25 MHz step resolution. During each scan, the cell temperature, HD partial pressure and baseline were slowly evolving, due to thermo-mechanical stress. Before being analyzed by the line fitting routine, the four interlaced spectra were independently corrected from a linear baseline before being recombined. This allows for partial compensation of baseline fluctuations related to temperature instability.

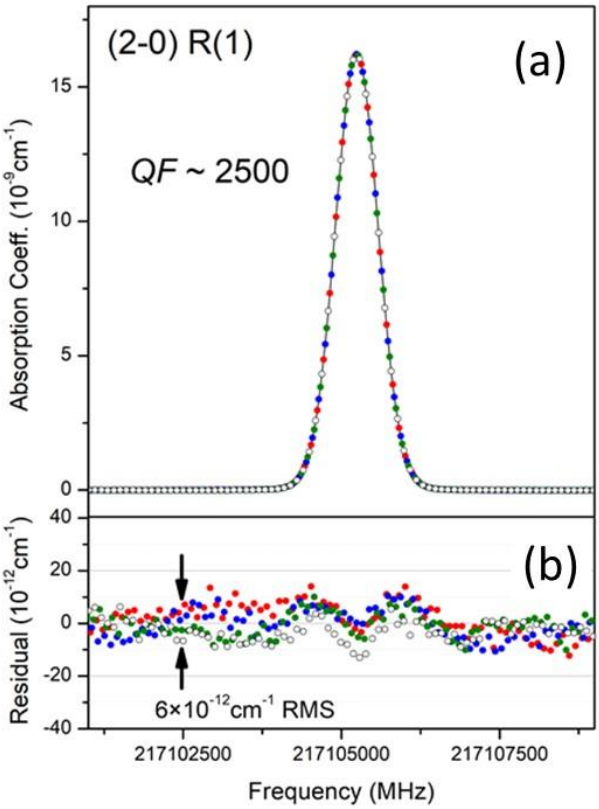

FIG. 2.
The (2-0) *R*(1) line of HD at liquid nitrogen temperature and a pressure of about 2 Pa.
(a) Typical fourfold interlaced spectra measured at liquid nitrogen temperature and at a pressure of 2 Pa. The four interlaced spectra are plotted with different colors and provide a 25 MHz step resolution while the cavity free spectral range is about 100 MHz. The black trace represents the fit of this line using a Voigt line profile (see text), (b) Residuals of the simultaneous fit of the four interlaced spectra. The noise equivalent absorption coefficient, α_{min}, evaluated from the baseline fluctuations is about 6×10^{-12} cm^{-1} leading to a quality factor of 2500.

Each of the eighty-three fourfold interlaced spectra were fitted independently. The line shape was chosen as a Voigt profile with the Gaussian width fixed to its 77 K Doppler value (770 MHz FWHM). The Lorentzian component width was fixed to 11 MHz to minimize the residuals. This width value has been determined by averaging the results of an initial fit for which this parameter was kept free. This weak component helps to account for a small temperature gradient existing in the probed gas sample, as detailed below for the *R*(0) line treatment. The center and area of the HD *R*(1) line as well as a quadratic baseline were determined by the fit. A typical fourfold spectrum together with the corresponding fit residuals are presented on **Fig. 2**. The root mean square (RMS) of the residuals (or noise equivalent absorption coefficient) is on the order of 6×10^{-12} cm^{-1} which leads to a quality factor of about 2500 (QF is defined as the ratio of the absorption coefficient at the peak to the RMS of the residuals).

The averaged value of the 83 center determinations of the (2-0) *R*(1) line is found to be 217105181934 kHz with a 1σ statistical deviation of 53 kHz. The Allan deviation plot of the retrieved frequencies, presented in **Fig. 3,** suggests that the accuracy of the averaged line center is below the RMS value but higher than the standard error ($\sigma/\sqrt{N} = 53/\sqrt{83} \approx 6$ kHz). The Allan deviation trace is going down, below 20 kHz, indicating that the average transition frequency value remains stable beyond this

limit. A 20 kHz value seems a conservative estimate of the actual uncertainty on the obtained line center value.

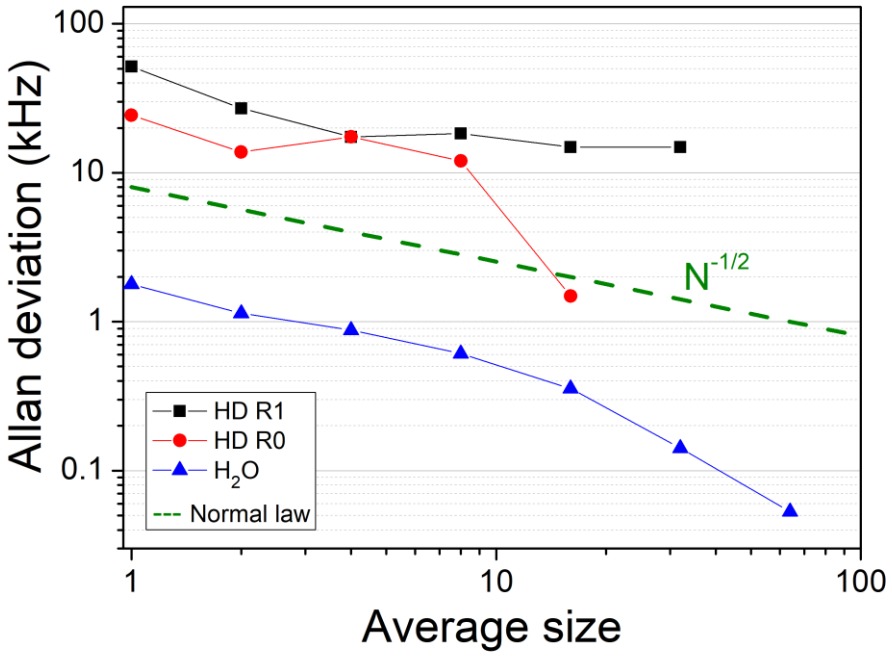

FIG. 3.
Allan deviation plot for the frequency determination of the $R(1)$, $R(0)$ HD lines and the (101)-(000) 2_{11}-3_{12} line of $H_2{}^{16}O$. The dataset size is 83, 33 and 247, respectively. The dependence is close to the normal law (in $1/\sqrt{N}$, green dashed line) for the water line leading to an error bar of about100 Hz for the Lamb-dip measurement. In the case of the $R(1)$ and, $R(0)$ line centers, the statistics help to decrease the error bar below a 20 kHz conservative value.

The R(0) line

For the more intense (2-0) $R(0)$ line, we recorded a series of 33 spectra. As said above, at 77 K, the $R(0)$ line intensity is increased by a factor of 3 compared to its room temperature value while the $R(1)$ line intensity is mostly unchanged. The cryogenic temperature of the cell allowed for a drastic reduction of the water contamination which is major issue. The (101)-(000) 2_{11}-3_{12} $H_2{}^{16}O$ line at 7168.4369 cm^{-1} has indeed a 1.196×10^{-20} cm/molecule intensity at room temperature and overlaps the profile of the $R(0)$ HD line at 7168.4703 cm^{-1} (with a room temperature intensity of 2.445×10^{-25} cm/molecule) [36].

Still, as evidenced in the following analysis of the $R(0)$ line profile, water traces persist, that we attribute to outgasing from the mirrors which are not cooled (see **Fig. 1** and [32], [33]) and remain at a temperature close to the room temperature. As shown below, the contribution of the water line to the observed absorption remains very weak but is detectable at the achieved sensitivity. In order to accurately constrain its position in the fitting of the $R(0)$ line profile, we determined the center of the interfering water line in saturated regime at room temperature, as shown in **Fig. 4**. A series of 247 spectra was recorded over 39 hours in order to refine the dip position. The reader is referred to [29] for the description of the acquisition of the line profile and Lamb dip spectra with adaptive resolution. Briefly, a first low resolution (100 MHz) survey scan was recorded, from which the line center was roughly

determined using a Gaussian profile. This spectrum was immediately supplemented with a high resolution (20 kHz) scan around the center as presented in the inset of **Fig. 4**. No effort was made to fit the ring-down using an advanced model (see *e.g.* [37]) and a Lorenzian fit was performed to determine the center of the Lamb dip. From the 247 determinations, an average center value of 214904329.8263(15) MHz or 7168.43683327(5) cm^{-1} was determined *i.e.* about 6.6 $\times 10^{-4}$ cm^{-1} below the HITRAN value provided with a 10^{-3} cm^{-1} error bar [36].

The Allan deviation included in **Fig. 3** indicates that the water line position is determined with 1.5 kHz accuracy per scan and that the precision is enhanced by the averaging process following the normal law in $1/\sqrt{N}$, where N is the number of recordings. The resulting standard error is thus decreased by a factor of about 15 ($\approx\sqrt{243}$) compared to the RMS leading to a very small uncertainty value of 0.1 kHz. This confirms the stability of the frequency detection chain. Note that the room temperature water line at 10^{-3} Pa pressure and the 80 K HD line at 2 Pa have similar peak absorption (about 15×10^{-9} cm^{-1}) and linewidths (627 and 770 MHz FWHM, respectively), but the water dip is remarkably deep (5×10^{-9} cm^{-1}) and much narrow (600 kHz FWHM). As a result, a gain of an order of magnitude is achieved in pointing the line center in saturation regime.

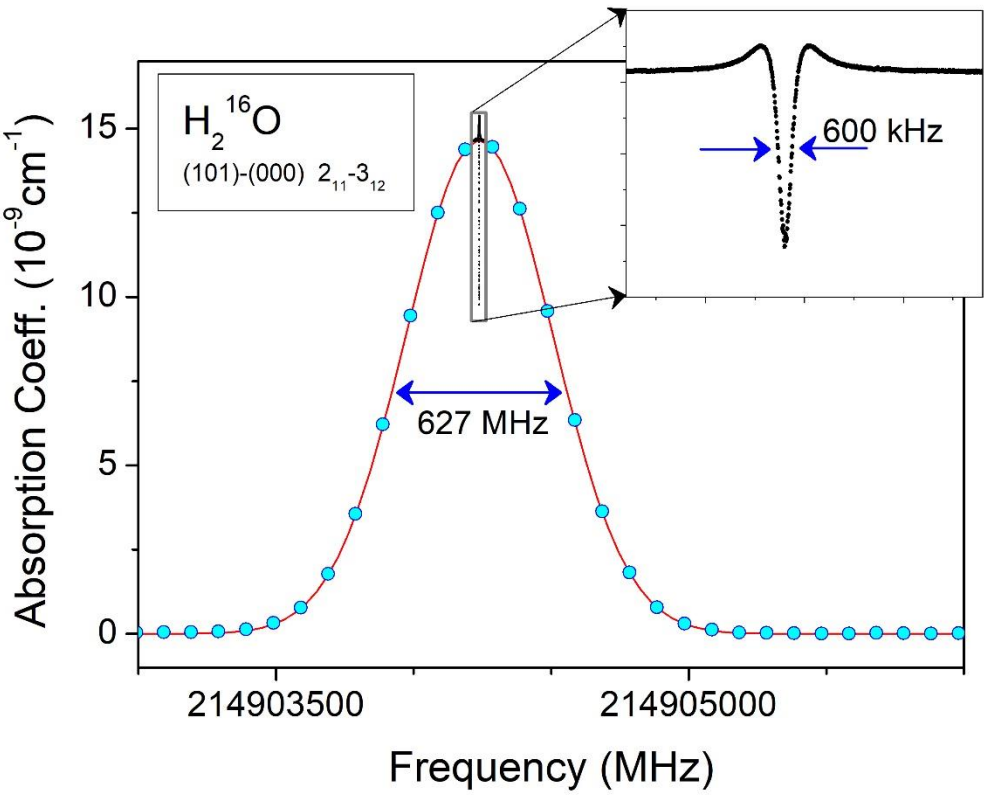

FIG. 4.
Room temperature line profile and Lamb dip of the water line, namely (101)-(000) 2_{11}-3_{12} of $H_2{}^{16}O$, interfering with the profile of the (2-0) $R(0)$ line of HD. A first low resolution (100 MHz) survey scan (blue dots) is recorded, from which the line center is roughly determined using a Gaussian profile (red line). The spectrum is supplemented with a high resolution (20 kHz) scan around the center (see inset). The center of Lamb dip determined is determined with a kHz accuracy from a single scan: 214904329.8263(15) MHz.

Following the same treatment as described for the *R*(1) line, the thirty-three fourfold interlaced spectra of the *R*(0) line were fitted with a Voigt profile with 77 K Doppler width and an effective Lorentzian width of 4 MHz (this value is an averaged value obtained after a first fit session in which the Lorentzian width was kept free). In **Fig. 5**, we present one of the 33 fitted spectra with the corresponding residuals. The residuals (blue trace) show an asymmetry which is interpreted as due to the above water line and may affect the determination of the *R*(0) line center. To minimize this effect, a weak water line contribution was added in the fit procedure. The center of the water line was fixed at its Lamb dip value (dashed vertical line in **Fig. 5**). The profile was taken as a Doppler profile corresponding to a temperature of 300K and the amplitude was adjusted. As a result, a symmetric residual is obtained (red trace). The fit RMS of a single spectrum is evaluated to 4×10^{-12} cm^{-1} leading to a quality factor of about 8500.

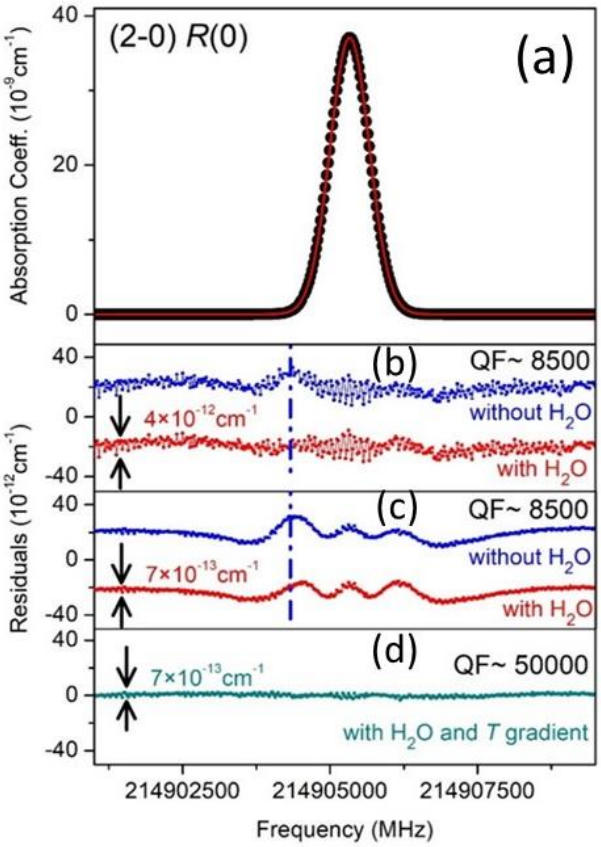

FIG. 5.
The (2-0) *R*(0) HD line at liquid nitrogen temperature and a pressure of about 2 Pa.
(a) Averaged spectrum (33 acquisitions, black dots) at a pressure of 2 Pa and corresponding best fit profile (red line),
(b) Residuals obtained from a fit of one of the thirty-three fourfold interlaced spectra, including or not the water line (red and blue points, respectively). The water line position is indicated by the vertical blue dashed line,
(c) Residuals obtained for the averaged spectrum including or not the water line (red and blue points, respectively)- see text for details,
(d) Residuals obtained for a simulation of the *R*(0) line as the sum of four different Doppler profiles at 77, 82, 218 and 275 K centered at the value previously determined and with fitted relative area of 84.6%, 14.3%, 1.1% and 0.1%, respectively. The water line is included in the fit with its position fixed to its Lamb dip value.

Averaging the 33 determinations of the center of the (2-0) $R(0)$ line leads to a value of 214905335220 kHz with a 1σ statistical deviation of 29 kHz. The Allan-variance plot of the line position series included in **Fig. 3**, confirms the absence of an obvious frequency determination drift over time. Although the number of recordings is limited, the statistics allows for a gain compared to the RMS value. In order to be conservative, we adopted the same 20 kHz uncertainty value as for the $R(0)$ line.

To validate our approach and better reveal the water line contribution in the baseline noise, we averaged together the 33 individual spectra to produce a single spectrum with improved signal-to-noise ratio. We fitted this spectrum by adjusting exclusively the line area, the line position and widths being fixed to their above values. The residuals included in **Fig.5** illustrate the gain on the S/N ratio (the trace thickness is decreased to about 7×10^{-13} cm^{-1}) and the water line is then clearly visible. It is interesting to note that the water line is very weak (10^{-11} cm^{-1} peak absorption *e.g.* one order of magnitude stronger than the noise level) but it shifts the fitted value of the HD line center by about 3 kHz because it slightly distorts the HD line profile. Let us emphasize that the averaged spectrum only served to confirm the contribution of the water line and validate the position parameter obtained from the 33 single fit determinations.

A clear symmetric structure remains in the residuals of our best fit (including the water line). We interpret this structure as a consequence of a temperature gradient due to the mirrors which are kept at room temperature and in contact with the gas. The effects of this gradient was revealed in spectra of methane at 80 K recorded with a similar cryogenic cell [38]. The relative population of high rotational energy levels of methane was found significantly larger than expected from the Boltzmann distribution at 80 K]. To test this interpretation, the continuous gradient of temperatures was modeled by four zones of decreasing sizes and increasing temperatures (77, 82, 218 and 275 K). It appears then that the profile of the HD line can be reproduced at the noise level limit by a sum of four Doppler profiles, corresponding to 77, 82, 218 and 275 K, with center fixed at the above-determined HD frequency, and a relative weight to the total area of 84.6, 14.3%, 1.1% and 0.1%, respectively. In this way, the symmetric structure remaining in the residuals vanishes (see lowest panel of **Fig. 5**) and the quality factor reaches a value of 50000. Even if based on a rough approximation, this result confirms that the linewidth is largely dominated by temperature rather than collisional effects that would affect the line center. The Lorentzian component used in the global fit procedure of the individual spectra is only an approximate solution which has the advantage of preserving the symmetry of the profile.

Transition frequencies and comparison with literature

Transition frequencies and error budget

The line center frequencies of the HD (2-0) $R(0)$ and $R(1)$ along with the one of the (101)-(000) 2_{11}-3_{12} H_2O transition are listed in **Table 1**. After correcting those frequencies by the recoil, the second order Doppler effect and the pressure shift, we obtain absolute transition frequencies of

217105181898(20) and 214905335185(20) kHz for the (2-0) $R(1)$ and $R(0)$ HD transitions respectively and 214904329820.80(10) kHz for the $H_2{}^{16}O$ (101)-(000) 2_{11}-3_{12} transition.

The $R(1)$ pressure shift correction was calculated using the pressure-shift coefficient of -0.87±0.05 kHz/Pa determined in [19] for the $R(1)$ transition. It leads to a correction of 1.74(1) kHz for our line center measured at 2 Pa. As concerns the $R(0)$ transition, in absence of literature value, we adopted the pressure shift coefficient of the $R(1)$ transition with a very conservative relative uncertainty of 50 % (pressure shifts coefficients measured for H_2 transitions do not show important rotational dependence [38], [39]). The frequency calibration chain is expected to bring no bias.

Table 1

Determination of the zero-pressure frequency and uncertainty (σ) contributions in kHz for the (2-0) $R(1)$ and $R(0)$ transitions of HD and for the (101)-(000) 2_{11}-3_{12} transition of H_2O.

	HD (2-0) $R(1)$		HD (2-0) $R(0)$		$H_2{}^{16}O$ (101)-(000) 2_{11}-3_{12}	
Number of recordings	83		33		243	
	Value (kHz)	σ *(kHz)*	Value (kHz)	σ *(kHz)*	Value (kHz)	σ *(kHz)*
Measured line center	217105181934	53/20 [a]	214905335220	29/20 [a]	214904329826.33	1.5/0.1 [a]
Pressure shift [b]	-1.74	0.1	-1.74	0.9	≈ 0	≈ 0
Quadratic Doppler effect	0.25	0	0.25	0	0.16	
Recoil	-34.62		-33.92		-5.69	
Transition frequency	217105181898	53/20 [a]	214905335185	30/21 [a]	214904329820.80	1.5/0.1 [a]

Notes

[a] *The first value is the RMS of the different determinations. The second value is the reduced value allowed by the statistics (see text),*

[b] *The R(1) pressure shift of -0.87(5) kHz/Pa was taken from [19] for the R(1) transition and assumed to be identical for the R(0) transition (see text).*

From **Table 1**, it appears that for the three considered lines, the overall uncertainty on the transition frequency is largely dominated by the line (or dip) center determination. Due to the low pressure of our recordings (2 Pa for HD and ~10^{-3} Pa for H_2O), the impact of the pressure shift is mostly negligible. In **Table 1**, we give for the different transitions the RMS deviation of the different determinations together with a (lower) error value resulting of the statistics of the recordings (N= 83, 33 and 243 recordings for $R(1)$, $R(0)$ and $H_2{}^{16}O$, respectively). In the case of the water line, the Allan deviation plot (**Fig. 3**) show that the statistics follows a normal law and the final uncertainty of about 100 Hz coincides with standard deviation. As discussed above, in the case of the $R(1)$ and $R(0)$ transitions of HD, the $1/\sqrt{N}$ trend is less obvious and, on the basis of **Fig. 3**, we give a 20 kHz uncertainty value as a conservative estimate of the real error bar.

Another possible source of error, not mentioned in **Table 1,** is related to the underlying hyperfine structure (hfs) of the $R(1)$ and $R(0)$ lines. The hfs structure of HD lines has been modeled in the literature by *ab initio* calculations [4] and a combination of *ab initio* calculations, an effective Hamiltonian and tensorial algebra [21]. The influence of the hfs on the pressure shift value and on the frequency determination of the (2-0) $R(1)$ was discussed in [19]. In the above profile analysis, the effect of the hfs was neglected considering it to be barycentric. In order to evaluate quantitatively the error associated to

this approximation, we first calculated the hfs of the (2-0) *R*(0) and (2-0) *R*(1) transitions using the parameters provided in [21] and changing the sign of some of them as mentioned in [18]. Other spectroscopic parameters were obtained from a global fit including experimental data concerning the *v*= 0 [11], [40] and *v*= 2 [25], [12], [17] states. Eigenvalues and relative intensities were evaluated using the PGOPHER software [41]. Simulations were performed by convolving the resulting stick spectra (**Fig. 6**) with a Gaussian profile. A series of simulated spectra were obtained by varying the full width at half maximum (FWHM) between 10 kHz and 30 MHz. The result of the overall profile was then fitted with a single Gaussian whose center, FWHM and area were adjusted. The differences between the line center of the Gaussian fit and the hfs-free transition frequency are plotted in **Fig. 6** *versus* the FWHM value used for the convolution. It appears that the apparent line center frequency is systematically smaller than the hfs-free transition frequency but the impact is very small for Gaussian widths larger than 1 MHz. The two considered HD lines have a Doppler broadening at 77 K of about 770 MHz making the impact of the hfs on the line profile totally negligible, as could have been expected from the spectral extension of the hfs (on the order of ±200 kHz) compared to the Doppler width. Note that the negligible impact of the hfs and possible associated cross-overs is an advantage for measurements in Doppler regime at low optical power regime.

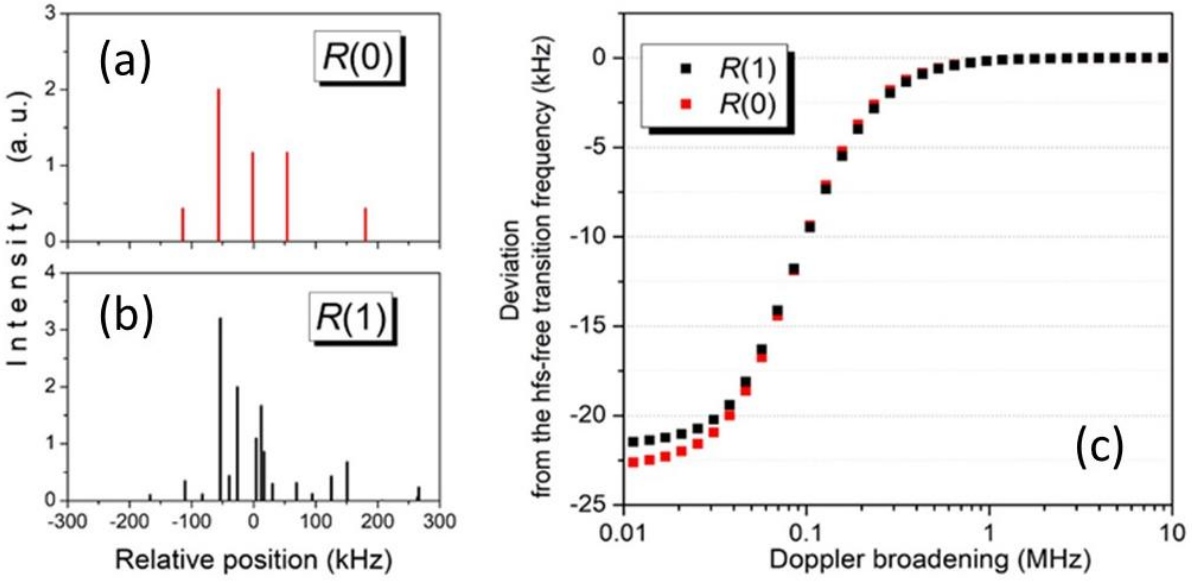

FIG. 6.
Impact of the hyperfine structure on the line center determination.
(a) (b) Calculated hfs of the (2-0) *R*(0) and *R*(1) transitions of HD, (c) Deviation of the apparent line center from the hfs-free transition frequency as a function of the FWHM of the Gaussian profile used to convolve the hfs (see text).

Comparison with literature

In **Figure 7** and **Table 2**, our (2-0) *R*(1) transition frequency is compared with the most precise measurements available to date. As mentioned above, the Hefei [26], and Amsterdam [16] values were

obtained in saturation regime while the Caserta value [19] relies on recordings in Doppler regime, as in the present work, but at room temperature. The four determinations are consistent. In particular, our value is only 3 kHz below the identical values measured in Amsterdam and Caserta, a difference about twenty times smaller than the error bars of the Amsterdam and Caserta studies (50 and 76 kHz, respectively).

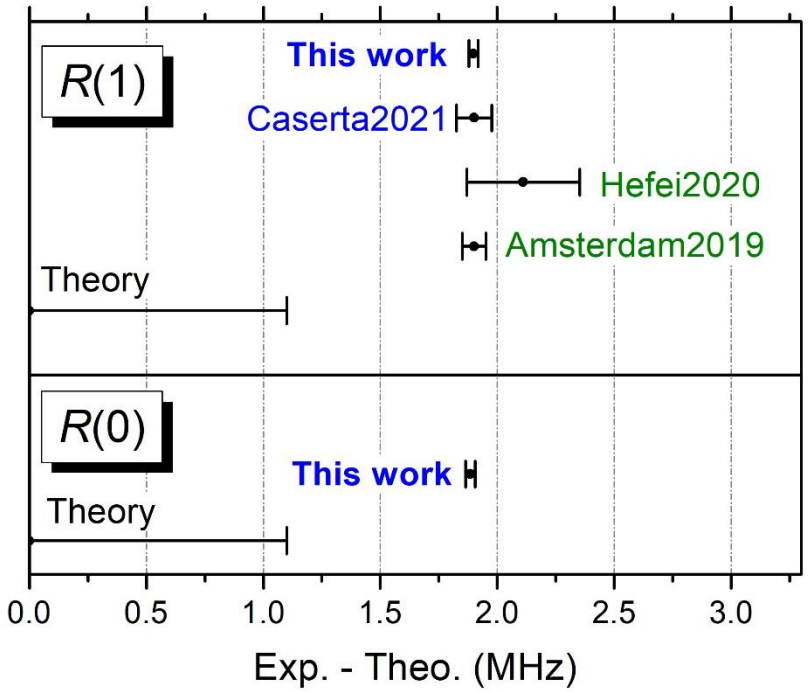

FIG.7
Comparison between the most recent experimental frequencies determination, in MHz, for the $R(1)$ and $R(0)$ transitions of the (2-0) vibrational band of HD. Amsterdam2019 refers to [16], Hefei2020 to [26], Caserta2021 to [19]. References related to measurements in Doppler regime or by saturation spectroscopy are indicated in blue and green, respectively. The origin of the frequency scale is the frequency evaluated theoretically from the H2spectre software detailed in [3] (see **Table 2**).

Table 2
Comparison between the most recent experimental and theoretical frequencies determination, in MHz, for the $R(0)$ and $R(1)$ transitions of the (2-0) vibrational band.

	$R(1)$	$R(0)$
Grenoble 2011 [12]	217 105 192(30)	214 905 315(30)
Amsterdam 2019 [16]	181.901(50)	
Hefei 2020 [26]	182.111(241)	
Caserta 2021 [19]	181.901(76)	
This work	**217 105 181.898(20)**	**214 905 335.185(20)**
Theory [3]	180.0(1.1)	333.3(1.1)

The frequency of the (2-0) $R(0)$ transition is consistent with the previous determination of [12] reported with a 30 MHz uncertainty. The uncertainty value is presently reduced by three orders of magnitude.

We have also included in **Table 2** the transition frequency provided by theory (values were computed using the H2spectre software detailed in Ref. [3]). These calculated values were used as

frequency origins in **Fig. 7**. For both for the *R*(0) and *R*(1) transitions, theoretical values are underestimated by about 1.88 MHz, what represents 1.7 times their claimed error bar (1.1 MHz). A similar deviation was already reported for the (2-0) *P*(1), *R*(2), *R*(3) lines measured with sub-MHz accuracy in Doppler-free regime [25], [17]. The mean deviation is of 1.91 MHz with a standard deviation of only 25 kHz for the five transitions, *P*(1) and *R*(0-3).

Conclusion

The (2-0) *R*(0) and *R*(1) transition frequencies have been determined in Doppler regime with an accuracy of 20 kHz (relative accuracy of about 10^{-10}). This level of accuracy was made possible by combining a very stable and coherent laser source, an absolute calibration of the frequency scale and the sensitivity of the CRDS technique, together with a liquid nitrogen cooled cell. The latter permitted to decrease Doppler transition linewidth and spectra contamination by water lines.

Indeed, up to now, the spectral interference with a water line had hampered high accuracy transition frequency measurements of the *R*(0) transition. The accuracy of the reported *R*(0) transition frequency represents a gain by three orders of magnitude compared to literature. The analysis of the *R*(0) line profile benefited of the accurate determination of the transition frequency of the (101)-(000) 2_{11}-3_{12} interfering line of $H_2{}^{16}O$, from separate recordings performed in saturation regime. A series of 247 Lamb dips were recorded, each scan providing a 1.5 kHz accuracy on the Lamb dip center determination. The Allan deviation indicates that the obtained dip centers follow the normal law, the final precision is enhanced to about 100 Hz. This level of accuracy (relative uncertainty of 5×10^{-13}) is at the state-of-the-art for molecular transition frequencies [42], [43], [44].

In the case of the *R*(1) transition of HD, our accuracy is at the level of the best previous determinations both in saturation regime and in Doppler regime. Note that the only accurate determination in Doppler regime was obtained from room temperature spectra recorded with pressures between 100 and 1500 Pa [19]. The sensitivity of the CRDS set-up used in the present work allowed us to record spectra at a significantly smaller pressure of 2 Pa which simplified the line profile analysis and made the self-pressure shift of the line center almost negligible.

The obtained results extend the set of accurate transition frequencies in the first overtone band of HD. The comparison to the most recent theoretical values [3] shows a systematic underestimation of 1.9 MHz of the calculated transition frequencies compared to the five accurate values at disposal, *P*(1) and *R*(0-3). This observation provides a challenge for future refinement of the non-adiabatic perturbation theory or any other theory applied to HD.

Conflicts of interest

There are no conflicts to declare.

Acknowledgments

S. K. thanks the REFIMEVE consortium (Equipex REFIMEVE+ ANR-11-EQPX-0039). C. L. thanks the Action de Recherches Concertées (Grant No. ARC iBEAM-18/23-090) and the Fonds de la

Recherche Scientifique (FNRS) for Grant No J.0129.20 and IISN Grant No. 4.4504. C. L. also thanks the CNRS for funding a research stay in Grenoble.

References

[1] L. Wolniewicz, *J. Chem. Phys.*, 1995, **103**, 1792.

[2] K. Pachucki and J. Komasa, *Phys. Chem. Chem. Phys.*, 2010, **12**, 9188.

[3] J. Komasa, M. Puchalski, P. Czachorowski, G. Łach, and K. Pachucki, *Phys. Rev. A*, 2019, **100**, 032519.

[4] J. Komasa, M. Puchalski, and K. Pachucki, *Phys. Rev. A*, **102**, 012814 (2020).

[5] G. Herzberg, *Nature*, 1950, **166**, 563.

[6] R.A. Durie and G. Herzberg, 1960, *Can. J. Phys.*, **38**, 806.

[7] P. J. Brannon, C. H. Church, and C. W. Peters, *J. Mol. Spectrosc.*, 1968, **27**, 44.

[8] A. McKellar, W. Goetz, and D. Ramsay, *Astrophys. J.*, 1976, **207**, 663.

[9] F. Dalby and J. Vigué, *Phys. Rev. Lett.*, 1979, **43**, 1310.

[10] N.H. Rich, J. Johns, and A.R. McKellar, *J. Mol. Spectrosc.*, 1982, **95**, 432.

[11] B. J. Drouin, S. Yu, J.C. Pearson, and H. Gupta, *J. Mol. Struct.*, 2011, **1006**, 2.

[12] S. Kassi and A. Campargue, *J. Mol. Spectrosc.*, 2011, **267**, 36.

[13] D. Sprecher, C. Jungen, W. Ubachs, and F. Merkt, *Faraday Disc.*, 2011, **150**, 51.

[14] S. Vasilchenko, D. Mondelain, S. Kassi, P. Čermák, B. Chomet, A. Garnache, S. Denet, V. Lecocq, and A. Campargue, *J. Mol. Spectrosc.*, 2016, **326**, 9.

[15] L.-G. Tao, A.-W. Liu, K. Pachucki, J. Komasa, Y. Sun, J. Wang, and S.-M. Hu, *Phys. Rev. Lett.*, 2018, **120**, 153001.

[16] M. L. Diouf, F. M. J. Cozijn, B. Darquié, E. J. Salumbides, and W. Ubachs, *Opt. Lett.*, 2019, **44**, 4733.

[17] M. Diouf, F. Cozijn, K.-F. Lai, E. Salumbides, and W. Ubachs, Phys. Rev. Res., 2020, **2**, 023209.

[18] A. Fast and S.A. Meek, *Phys. Rev. Lett.*, 2020, **125**, 023001.

[19] A. Castrillo, E. Fasci, and L. Gianfrani, *Phys. Rev. A*, 2021, **103**, 022828.

[20] J. Komasa, K. Piszczatowski, G. Łach, M. Przybytek, B. Jeziorski, and K. Pachucki, *J. Chem. Theory Comput.*,2011, **7**, 10 3105.

[21] P. Dupré, *Phys. Rev. A*, 2020, **101**, 022504.

[22] H. Jóźwiak, H. Cybulski, and P. Wcisło, *J. Quant. Spectrosc. Radiat. Transfer*, 2021, **272**, 107753.

[23] D. Sprecher, J. Liu, C. Jungen, W. Ubachs, and F. Merkt, *J. Chem. Phys.*, 2010, **133**, 111102.

[24] G. D. Dickenson, M. L. Niu, E. J. Salumbides, J. Komasa, K. S. Eikema, K. Pachucki, and W. Ubachs, *Phys. Rev. Lett.*, 2013, **110**, 193601.

[25] F. M. Cozijn, P. Dupré, E. J. Salumbides, K. Eikema, and W. Ubachs, *Phys. Rev. Lett.*, 2018, **120**, 153002.

[26] T.-P. Hua, Y. Sun and S.-M. Hu, *Opt. Lett.* 2020, **45**, 4863.

[27] Y.-N. Lv, A.-W. Liu, Y. Tan, C.-L. Hu, T.-P. Hua, X.-B. Zou, Y. R. Sun, C.-L. Zou, G.-C. Guo, and S.-M. Hu, 2022, arXiv:2203.12240.

[28] J. Burkart, D. Romanini, and S. Kassi, Opt. Lett., 2014, **39**, 4695.

[29] S. Kassi, T. Stoltmann, M. Casado, M. Daëron, and A. Campargue, *J. Chem. Phys.*, 2018, **148**, 054201.

[30] M. Casado, T. Stoltmann, A. Landais, N. Jobert, M. Daëron, F. Prié, and S. Kassi, *Applied Physics B*, 2022, **128**, 58.

[31] N. Jobert, M. Casado, and S. Kassi, *Appl. Phys. B*,2022 **128,** 56.

[32] S. Kassi, B. Gao, D. Romanini, and A. Campargue, *Phys. Chem. Chem. Phys.*, 2008, **10**, 4410.

[33] S. Kassi, D. Romanini, and A. Campargue, *Chem. Phys. Lett.*, 2009, **477**, 17.
[34] L. Wang, S. Kassi, A. Liu, S. Hu, and A. Campargue, *J. Quant. Spectrosc. Radiat. Transfer*, 2011, **112**, 937.
[35] D. Mondelain, S. Kassi, L. Wang, and A. Campargue, *Phys. Chem. Chem. Phys.*, 2011, **17**, 7985.
[36] I.E. Gordon, L.S. Rothman, R.J. Hargreaves, R. Hashemi, E.V. Karlovets, F.M. Skinner, E.K. Conway, C. Hill, R.V. Kochanov, Y. Tan, P. Wcislo, A.A. Finenko, K. Nelson, P.F. Bernath, M. Birk, V. Boudon, A. Campargue, K.V. Chance, A. Coustenis, B.J. Drouin, J.–M. Flaud, R.R. Gamache, J.T. Hodges, D. Jacquemart, E.J. Mlawer, A.V. Nikitin, V.I. Perevalov, M. Rotger, J. Tennyson, G.C. Toon, H. Tran, V.G. Tyuterev, E.M. Adkins, A. Baker, A. Barbe, E. Canè, A.G. Császár, A. Dudaryonok, O. Egorov, A.J. Fleisher, H. Fleurbaey, A. Foltynowicz, T. Furtenbacher, J.J. Harrison, J.–M. Hartmann, V.–M. Horneman, X. Huang, T. Karman, J. Karns, S. Kassi, I. Kleiner, V. Kofman, F. Kwabia–Tchana, N.N. Lavrentieva, T.J. Lee, D.A. Long, A.A. Lukashevskaya, O.M. Lyulin, V.Yu. Makhnev, W. Matt, S.T. Massie, M. Melosso, S.N. Mikhailenko, D. Mondelain, H.S.P. Müller, O.V. Naumenko, A. Perrin, O.L. Polyansky, E. Raddaoui, P.L. Raston, Z.D. Reed, M. Rey, C. Richard, R. Tóbiás, I. Sadiek, D.W. Schwenke, E. Starikova, K. Sung, F. Tamassia, S.A. Tashkun, J. Vander Auwera, I.A. Vasilenko, A.A. Vigasin, G.L. Villanueva, B. Vispoel, G. Wagner, A. Yachmenev, and S.N. Yurchenko, *J. Quant. Spectrosc. Radiat. Transf.*, 2022, **277**, 107949.
[37] O. Votava, S. Kassi, A. Campargue, and D. Romanini, *Phys. Chem. Chem. Phys.*, 2022, **24**, 4157.
[38] A. Campargue, S. Kassi,K. Pachucki, J. Komasa, *Phys. Chem. Chem. Phys.*, 2012, 14(2), 802.
[39] S Kassi, A. Campargue, *J. Mol. Spectrosc.*, 2014, **300**, 55.
[40] L. Ulivi, P. De Natale, and M. Inguscio, *Astrophys. J.*, 1991, **378**, L29.
[41] C. M. Western and B. E. Billinghurst, *Phys. Chem. Chem. Phys.*, 2017, **19**, 10222.
[42] K. Bielska, S. Wójtewicz, P. Morzynski, P. Ablewski, A. Cygan, M. Bober, J. Domysławska, M. Zawada, R. Ciuryło, P. Masłowski, and D. Lisak, *J. Quant. Spectrosc. Radiat. Transfer*, 2017, **201**, 156.
[43] Z. D. Reed, D. A. Long, H. Fleurbaey, and J. T. Hodges, *Optica*, 2020, **7**, 1209.
[44] Z. D. Reed, B. J. Drouin, D. A. Long, J. T. Hodges, *J. Quant. Spectrosc. Radiat. Transfer.*, 2021, **271**, 107681.